Analysis of the Noise Voltage Coupling (Crosstalk) Between Right-Handed and Composite Right/Left-Handed (CRLH) Transmission Lines on Printed Circuit Boards

Irfanullah, *Member, IEEE*, Sanjay Nariyal, *Student Member, IEEE*, Sayan Roy, *Student Member, IEEE*, Muhammad Mubeen Masud, Bilal Ijaz, and Benjamin D. Braaten, *Member, IEEE*

***Abstract*—One aspect of the electromagnetic compatibility (EMC) analysis of RF circuitry is the accurate modeling of the coupling between printed transmission lines. Correct modeling of this coupling is essential because unwanted noise voltages can be substantial and create adverse effects on sensitive components. Recently, the development of composite right-/left-handed transmission lines (CRLHTLs) has received considerable attention due to the unique propagation characteristics. Because of this increase in applications, CRLHTLs are being implemented in RF systems with other printed circuitry, such as microstrip transmission lines, in very close proximity. In many of these instances, the coupling may not be intentional. To study this interaction between CRLHTLs and other printed circuitry from an EMC point of view, this paper presents derived analytical expressions for computing the near- and far-end voltage coupling between right-handed (printed microstrip transmission lines) and CRLHTLs. More specifically, these expressions are used to determine the near- and far-end voltages weakly coupled to the CRLHTL when the conventional microstrip right-handed transmission line is driven with a source and terminated with a load. These expressions are then used to illustrate how the induced voltages on the CRLHTL can be reduced by the capacitance and inductance values that support left-handed propagation. This can be a useful alternative to conventional shielding. Furthermore, design guidelines and tradeoffs are presented on the layout of CRLHTL near other printed transmission lines. The expressions derived in this paper are validated with simulations and measurements.**

***Index Terms*—Coupling, crosstalk and composite right-/left-handed transmission lines (CRLHTLs).**

I. Introduction

THE use of modern wireless communication systems is growing rapidly. The increasing functionality of wireless systems is requiring more RF electronic circuitry to be placed into a smaller area. To preserve the operating characteristics of this RF circuitry, it is essential that proper electromagnetic compatibility (EMC) analysis of the system is performed. Many new technologies for reducing the size of RF circuitry and improving the performance have been proposed by researchers and engineers. One of these technologies that has received considerable attention is the composite right-/left-handed transmission line (CRLHTL) [1]–[16] shown below the right-handed microstrip transmission (RHTL) line in Fig. 1(a). To achieve left-handed (LH) propagation, the equivalent circuit of the traditional microstrip RHTL in Fig. 1(a) is modified. In particular, instead of a series inductance and shunt capacitance to model the RHTL, the components are interchanged to give a circuit with a series capacitance and a shunt inductance. A schematic of the CRLHTL is shown in Fig. 1(b). The series capacitance that supports LH propagation is denoted as C_L and the shunt inductance that supports LH propagation is denoted as L_L. Two other components, L_R and C_R, are also introduced to represent the parasitic affects of the printed microstrip CRLHTL. In particular, L_R represents the parasitic

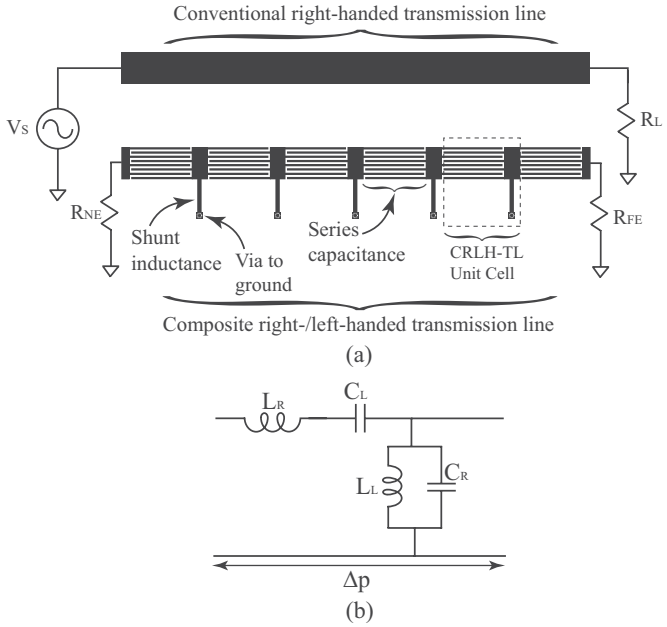

Fig. 1. (a) Coupled conventional RH and CRLHTLs and b) the equivalent circuit of a CRLHTL unit cell.

Manuscript received February 24, 2012; revised August 3, 2012; accepted October 18, 2012. Date of publication December 5, 2012; date of current version July 22, 2013.

The authors are with the Department of Electrical and Computer Engineering, North Dakota State University, Fargo, ND 58102 USA (e-mail: irfan.ullah@ndsu.edu; Sanjay.Nariyal@ndsu.edu; sayan.roy@ndsu.edu; muhammadmubeen.masud@ndsu.edu; bilal.ijaz@ndsu.edu; benbraaten@ieee.org).

Color versions of one or more of the figures in this paper are available online at http://ieeexplore.ieee.org.

Digital Object Identifier 10.1109/TEMC.2012.2226214

inductance of the CRLHTL introduced by current traveling down the TL and C_R is the parasitic capacitance between the printed conductors on top of the substrate and the ground plane. Therefore, for LH propagation on the CRLHTL, the values of C_L and L_L should dominate over the values of C_R and L_R. To introduce a series capacitance C_L along the CRLHTL, interdigitated capacitors are printed along the length of the transmission line. Also, to introduce a shunt inductance L_L, short-circuit stubs are attached along the length of the CRLHTL.

CRLHTLs have been used to develop novel compact printed antennas with better radiation efficiencies [1], compact power dividers with arbitrary coupling [3], [8], zero-phase transmission lines that are a fraction of a wavelength long [13], and flat lenses [16]. Because of these benefits, CRLHTLs will become more popular for RF circuit design. However, very little work has been done on CRLHTLs from an EMC analysis point of view.

For many of the aforementioned applications, LH propagation along the CRLHTL must be supported. As previously mentioned, to support this LH propagation, the effects of C_L and L_L along the transmission line should dominate the effects of C_R and L_R. Unfortunately, many of the analytical EMC computations presented in [17]–[19] to model the weak coupling between printed transmission lines using equivalent circuits are not sufficient for modeling the coupling between a conventional RHTL and a CRLHTL. Fortunately, there has been significant work on the coupling between microstrip RH to CRLHTLs presented in [2]–[4] and [7] and [8]. In this previous research, the coupling between the microstrip RH and CRLHTLs is assumed to be intentional and results on arbitrary coupling, impedances, and bandwidths are presented. However, for this paper, the coupling is assumed to be weak and unintentional and techniques to mitigate the unwanted coupling and design guidelines to reduce the coupling are presented. In summary, the objective of this paper is to study the unintentional weak coupling between the conventional RHTL and the CRLHTL shown in Fig. 1(a) for EMC and electromagnetic interference purposes.

Initially, the coupling problem is modeled with an equivalent circuit and analytical expressions for the near- and far-end voltages coupled to the CRLHTL from the RHTL are derived for a single unit cell. To validate these new expressions (and the equivalent circuit), a 7-unit-cell coupling problem is simulated in the full-wave electromagnetics software advanced design system (ADS) [20] and several prototype boards are manufactured and tested. Next, the analytical expressions are used to study how the near- and far-end voltages can be reduced by various values of C_L and L_L, which are used to support LH propagation on the CRLHTL. Finally, design guidelines for CRLHTLs are presented. In particular, tradeoffs between the LH-propagation frequency bands and coupled voltages are presented and spacing requirements between conventional RHTLs and CRLHTLs are outlined.

II. Analytical Derivations of the Near- and Far-End Voltages for Coupled RH and CRLHTLs

The layout of the coupled RH and CRLHTL unit cells is shown in Fig. 2(a). The problem consists of a RHTL with

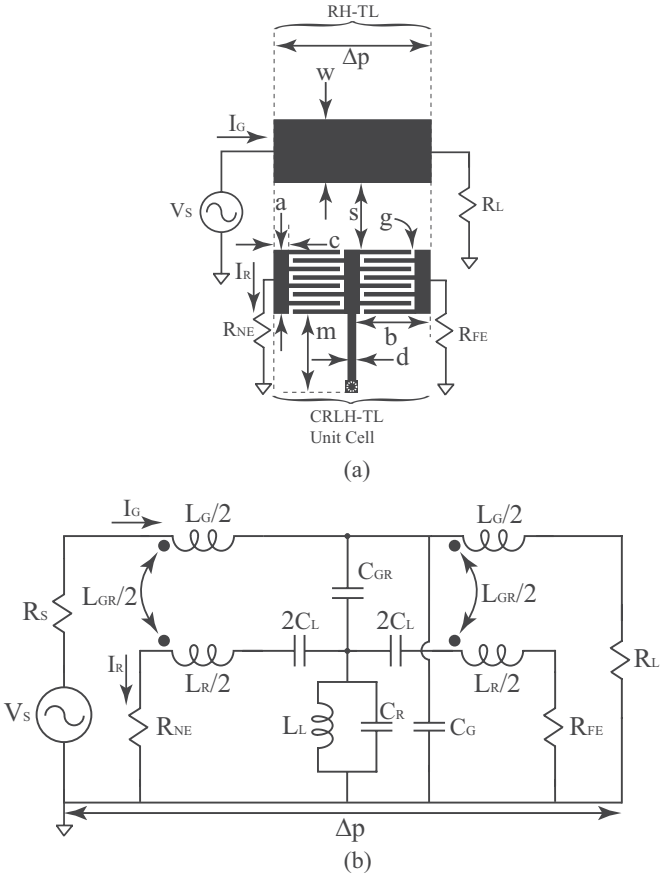

Fig. 2. (a) Unit cell of coupled RH and symmetric CRLHTLs and b) the equivalent circuit of the unit cell of coupled RH and symmetric CRLHTLs

a length of Δp and width w separated from a CRLHTL a distance s. The RHTL is driven with voltage source V_s and is terminated with a load resistance denoted as R_L. The CRLHTL is symmetrical and is loaded with a near-end resistance $R_{\rm NE}$ and a far-end resistance $R_{\rm FE}$. The RHTL with the source is referred to as the generator conductor and the CRLHTL with the near- and far-end resistance is referred to as the receptor conductor. The equivalent circuitry from the microstrip RH/CRLH couplers presented in [2] and [3] will be adopted for this paper. An equivalent circuit of the coupled unit cells in Fig. 2(a) is shown in Fig. 2(b) [2]. The inductance and capacitance of the generator conductor (RHTL) is denoted as L_G and C_G, respectively. The mutual inductance and capacitance between the generator and receptor conductors are denoted as $L_{\rm GR}$ and $C_{\rm GR}$, respectively. For the following derivations, the near- and far-end voltage will be derived for capacitive and inductive weak coupling. Then, the total coupling will be approximated by adding the contribution from both capacitive and inductive coupling [17].

A. Capacitively Coupled Transmission Lines

Initially, the coupling between the unit cell transmission lines in Fig. 2(a) will be evaluated for large values of R_L, $R_{\rm NE}$, and $R_{\rm FE}$. This then simplifies the general weak coupling circuit in Fig. 2(b) to the equivalent circuit in Fig. 3(a) which assumes that the coupling between the cells is dominantly capacitive. Next,

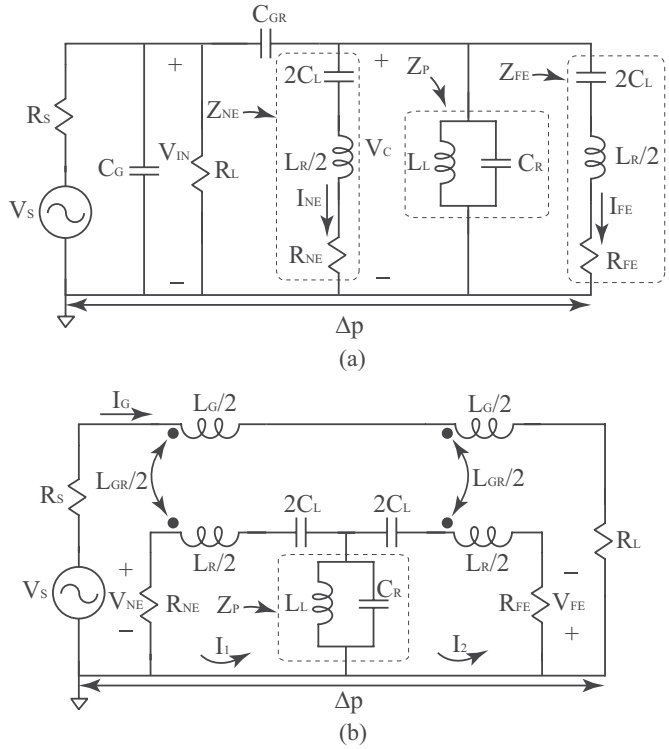

Fig. 3. (a) Equivalent circuit of capacitively coupled lossless RH and CRLHTLs and b) the equivalent circuit of inductively coupled lossless RH and CRLHTLs.

using voltage division, the coupled voltage V_c can be written as

$$V_c = V_{\text{in}} \frac{Z_{\text{eq}}}{Z_{\text{eq}} + Z_{\text{CGR}}} \tag{1}$$

where

$$Z_{\text{eq}} = \frac{Z_{\text{NE}} Z_{\text{FE}} Z_P}{Z_{\text{FE}} Z_P + Z_{\text{NE}} Z_P + Z_{\text{NE}} Z_{\text{FE}}} \tag{2}$$

$$Z_{\text{NE}} = R_{\text{NE}} + \frac{1}{2j\omega C_L} + \frac{j\omega L_R}{2} \tag{3}$$

$$Z_{\text{FE}} = R_{\text{FE}} + \frac{1}{2j\omega C_L} + \frac{j\omega L_R}{2} \tag{4}$$

$$Z_P = \frac{\frac{1}{j\omega C_R} j\omega L_L}{\frac{1}{j\omega C_R} + j\omega L_L} \tag{5}$$

$$Z_{\text{CGR}} = \frac{1}{j\omega C_{GR}} \tag{6}$$

and

$$V_{\text{IN}} \approx V_s \frac{R_L}{R_L + R_s}. \tag{7}$$

Then, the near-end voltage due to capacitive coupling can be written as

$$V_{\text{NE}}^{\text{CAP}} = R_{\text{NE}} \frac{V_c}{Z_{\text{NE}}}. \tag{8}$$

Similarly, the far-end voltage can be written as

$$V_{\text{FE}}^{\text{CAP}} = R_{\text{FE}} \frac{V_c}{Z_{\text{FE}}}. \tag{9}$$

Therefore, if $R_{\text{NE}} = R_{\text{FE}}$ then $V_{\text{NE}}^{\text{CAP}} = V_{\text{FE}}^{\text{CAP}}$. Closer observation of (8) and (9) shows that the near- and far-end voltages can be reduced by increasing Z_{NE} and Z_{FE}, respectively. This corresponds to decreasing the capacitance of the interdigital capacitors or the LH capacitance C_L on the CRLHTL.

B. Inductively Coupled Transmission Lines

Next, the coupling between the RH and CRLHTLs in Fig. 2(a) will be evaluated for small values of R_L, R_{NE}, and R_{FE}. This then simplifies the general coupling circuit in Fig. 2(b) to the equivalent circuit in Fig. 3(b) which assumes that the coupling between the cells is dominantly inductive. For this analysis, it is assumed that

$$I_G \approx \frac{V_s}{R_S + R_L}. \tag{10}$$

Then, using KCL around the left loop (loop 1) in the circuit in Fig. 3(b) gives

$$I_1 = \frac{I_2 Z_P + I_G Z_{\text{LGR}}}{Z_{\text{DNE}}} \tag{11}$$

where $Z_{\text{DNE}} = Z_{\text{NE}} + Z_P$ and $Z_{\text{LGR}} = j\omega L_{GR}/2$. Similarly, KCL around the right loop (loop 2) gives

$$I_2 = \frac{I_1 Z_P + I_G Z_{\text{LGR}}}{Z_{\text{DFE}}} \tag{12}$$

where $Z_{\text{DFE}} = Z_{\text{FE}} + Z_P$. Next, substituting (12) into (11) gives

$$I_1 = \frac{I_G Z_{\text{LGR}} (Z_P + Z_{\text{DFE}})}{Z_{\text{DFE}} Z_{\text{DNE}} - Z_P^2}. \tag{13}$$

Then, substituting (13) into (12) gives

$$I_2 = \frac{I_G Z_{\text{LGR}} (Z_P + Z_{\text{DNE}})}{Z_{\text{DFE}} Z_{\text{DNE}} - Z_P^2}. \tag{14}$$

Therefore,

$$V_{\text{NE}}^{\text{IND}} = I_1 R_{\text{NE}} \tag{15}$$

and

$$V_{\text{FE}}^{\text{IND}} = I_2 R_{\text{FE}}. \tag{16}$$

For the special case where $R_{\text{NE}} = R_{\text{FE}}$, then $V_{\text{NE}}^{\text{IND}} = V_{\text{FE}}^{\text{IND}}$.

C. Total Coupling Approximation Between the RH and CRLHTLs

Finally, the total weak coupling between the transmission lines can be approximated using the inductive–capacitive model [17]. In particular, the near- and far-end voltages can be approximated as the sum of the capacitive and inductive coupling in the following manner [17]:

$$V_{\text{NE}}^{\text{TOT}} = V_{\text{NE}}^{\text{CAP}} + V_{\text{NE}}^{\text{IND}} \tag{17}$$

and

$$V_{\text{FE}}^{\text{TOT}} = V_{\text{FE}}^{\text{CAP}} + V_{\text{FE}}^{\text{IND}}. \tag{18}$$

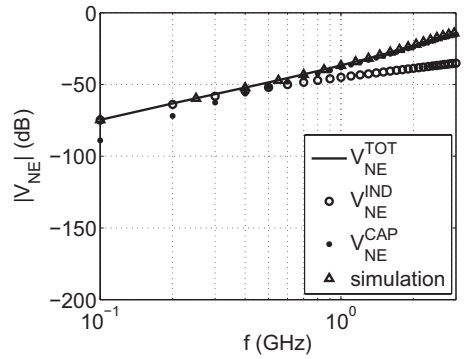

Fig. 4. Comparison of the analytical computations and circuit simulations of the general coupling circuit for $R_L = 20\,\Omega$.

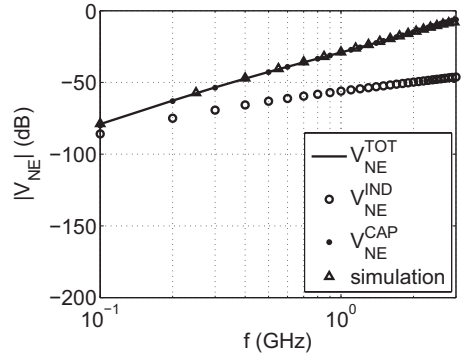

Fig. 5. Comparison of the analytical computations and circuit simulations of the general coupling circuit for $R_L = 200\,\Omega$.

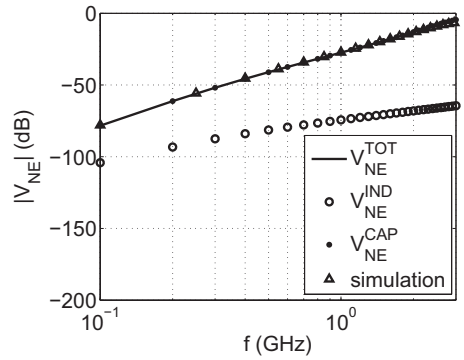

Fig. 6. Comparison of the analytical computations and circuit simulations of the general coupling circuit for $R_L = 2\,\mathrm{K}\Omega$.

To illustrate the accuracy of (17) and (18), the general coupling circuit in Fig. 2(b) was simulated in ADS for the following values [1]: $V_s = 1.0$ V, $R_s = 50\,\Omega$, $C_G = 0.33$ pF, $C_{GR} = 0.33$ pF, $L_R = 1.1$ nH, $C_R = 0.45$ pF, $L_L = 3.04$ nH, $C_L = 1.3$ pF, $L_{\mathrm{GR}} = 0.13$ nH, $L_G = 0.825$ nH, $R_{\mathrm{NE}} = 200\ \Omega$, and $R_{\mathrm{FE}} = 200\ \Omega$. These values were chosen to be similar to the RH-/CRLH-phase coupler in [1]. This ensured that noise voltages were coupled to the receptor in both the LH- and RH-propagating bands. These simulated values are then compared with the analytical computations using (17) in Figs. 4–6 for various values of R_L. Good agreement can be observed between the analytically computed total near-end voltages and the simulation values, showing the accuracy of the approximation in (17). It should also be mentioned that this accuracy was observed for both (17) and (18) for $R_{\mathrm{NE}} = R_{\mathrm{FE}} = 20\,\Omega$ (inductively dominant coupling) and $R_{\mathrm{NE}} = R_{\mathrm{FE}} = 2\,\mathrm{K}\Omega$ (capacitively dominant coupling).

D. Comparing the Inductive and Capacitive Coupling Terms

The results in Fig. 4 show that for frequencies below 500 MHz, the inductive coupling is dominant and for frequencies above 500 MHz, the capacitive coupling is dominant. This indicates that for frequencies $f < 500$ MHz, $V_{\mathrm{NE}}^{\mathrm{IND}}$ is dominant in (17) and for frequencies $f > 500$ MHz, $V_{\mathrm{NE}}^{\mathrm{CAP}}$ is dominant. This transition frequency can be determined by comparing the terms in (8) to (15). After several algebraic steps, it can be shown that the near-end transition frequency occurs when

$$\left|Z_{\mathrm{LGR}} Z_{\mathrm{CGR}}\right| \approx \left|\frac{R_L Z_{\mathrm{FE}} Z_P}{Z_{\mathrm{FE}} + 2Z_P}\right| \tag{19}$$

where the approximation $Z_{\mathrm{eq}} + Z_{\mathrm{CGR}} \approx Z_{\mathrm{CGR}}$ has been assumed. Notice that (19) is written in terms of the load and the far-end resistance values. Similar expression can be found in terms of the load and the near-end resistance values in [17] for the inductive and capacitive coupling between two printed TLs.

Several valuable comments can be made about (19). First, when designing the shielding of a CRLHTL against unintentional coupling, both inductive and capacitive shielding should be considered. Second, depending on the impedance values, there can exist certain bands where inductive coupling is dominant below a certain frequency f_1 and above a different frequency f_2 where $f_2 > f_1$. This means that capacitive coupling can be dominant over a certain finite band while inductive coupling exists in the remaining band. Finally, notice the transition frequency strongly depends on the load resistance R_L. Also, note that a similar expression to (19) can be derived for the far-end voltage.

III. Simulation and Measurement Validation Results

To validate the equivalent circuit model, the coupled transmission line problem shown in Fig. 1(a) was designed with 7 CRLH unit cells in the full-wave electromagnetics solver momentum [20], manufactured and tested. The transmission lines were printed on a 1.575-mm thick Rogers RT/duroid 5880 ($\varepsilon_r = 2.2$, $\tan\delta = 0.0009$) [21] substrate. Three different coupled transmission lines were printed. The ports not being measured were terminated with a 50 Ω. The first test case (case 1) manufactured is shown in Fig. 7(a), the second test case (case 2) manufactured is shown in Fig. 7(b), and the third test case (case 3) is shown in Fig. 7(c). The dimensions of each unit cell are shown in Fig. 7. Case 1 had an inductor stub length of $m = 4.75$ mm and a finger spacing between the interdigital capacitors of $g = 0.25$ mm. Case 2 had a longer shunt inductance of $m = 9.75$ mm with the same spacing between the interdigital capacitor fingers of $g = 0.25$ mm. Finally, case 3 had an inductive stub length similar to case 2 ($m = 8.85$ mm) while the spacing between the interdigital capacitor fingers was increased to $g = 0.35$ mm. Case 2 was used to investigate the accuracy of

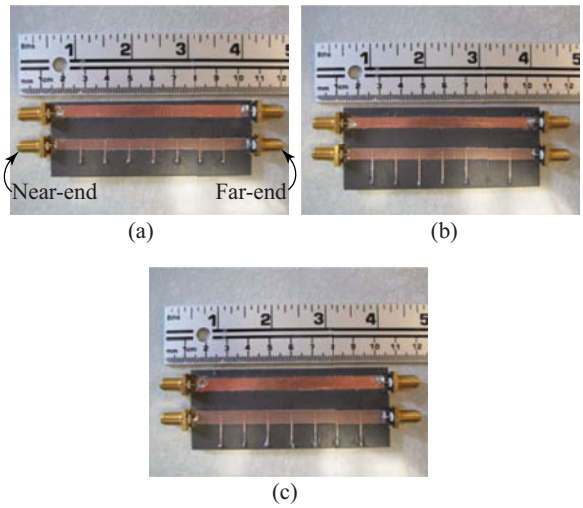

Fig. 7. (a) Picture of the manufactured 7-unit-cell RH-/CRLH-coupled transmission lines for case 1 (a = 5.25 mm, b = 10.4 mm, c = 0.5 mm, d = 0.5 mm, g = 0.25 mm, m = 4.75 mm, Δp = 21.42 mm, s = 10 mm, w = 4.8 mm); b) picture of the manufactured 7-unit-cell RH-/CRLH-coupled transmission lines for case 2 (a = 5.25 mm, b = 10.4 mm, c = 0.5 mm, d = 0.5 mm, g = 0.25 mm, m = 9.75 mm, Δp = 21.42 mm, s = 10 mm, w = 4.8 mm); c) picture of the manufactured 7-unit-cell RH-/CRLH-coupled transmission lines for case 3 (a = 6.15 mm, b = 10.4 mm, c = 0.5 mm, d = 0.5 mm, g = 0.35 mm, m = 8.85 mm, Δp = 21.42 mm, s = 10 mm, w = 5.7 mm).

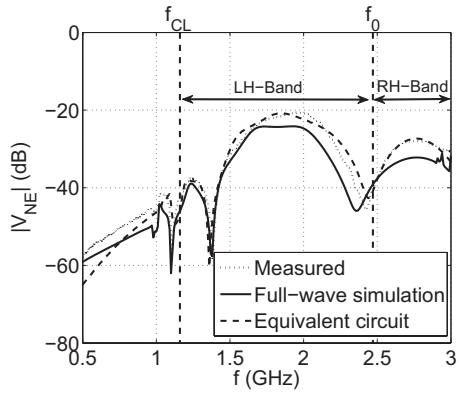

Fig. 8. Near-end voltage for case 1.

the equivalent circuit model for different values of shunt inductance and case 3 was used to show the accuracy of the model for different values of series capacitance. The measurements for all three cases are shown in Figs. 8–10. The near- and far-end coupling was measured using an Agilent ENA series network analyzer.

The equivalent circuit of each unit cell for cases 1, 2 and 3 were also extracted from the simulated *S*-parameters using the matrix method described in [1] and further optimized using designer [20]. The extracted equivalent circuit values are shown in Table I and the optimized values using designer are shown in Table II for direct comparison. The extracted values in Table I had an extraction frequency of f_0 (the RH-/LH-transition frequency). Each case of the coupled transmission lines was modeled in designer using 7 unit cells of the coupled transmission line circuit shown in Fig. 2(b). To model the measurement terminations in designer appropriately, R_L, $R_{\rm NE}$, and $R_{\rm FE}$ were

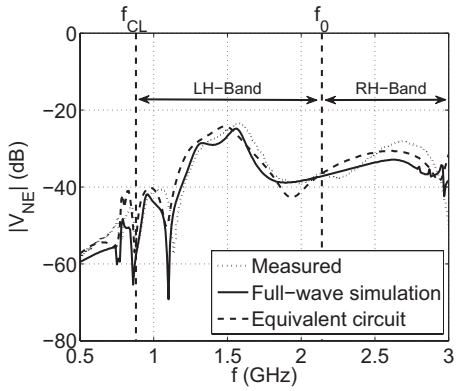

Fig. 9. Near-end voltage for case 2.

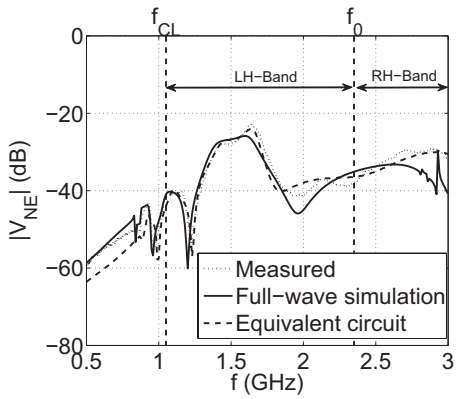

Fig. 10. Near-end voltage for case 3.

TABLE I
EXTRACTED EQUIVALENT CIRCUIT VALUES FOR THE COUPLED RH/CRLHTL UNIT CELLS

Value	Case 1	Case 2	Case 3
L_R (nH)	2.22	2.22	2.22
C_L (pF)	1.57	1.57	0.99
L_L (nH)	3.4	6.12	6.12
C_R (pF)	1.65	1.65	1.65
L_G (nH)	2.2	2.2	2.2
C_G (pF)	0.94	0.94	0.99
L_{GR} (nH)	0.059	0.059	0.089
C_{GR} (pF)	0.0274	0.0196	0.0117

all defined to be 50 Ω. The equivalent circuit results using the optimize values are shown to agree with measurements in Figs. 8–10.

Finally, the full-wave simulation tool momentum [20] was used to model all three measurement cases. The results from these simulations are also shown in Figs. 8–10 and computed nulls are within a few percent of the measured values. Overall, agreement between measurements, equivalent circuit simulations and full-wave simulations can be observed. This shows that the equivalent circuit in Fig. 2(b) can be used to accurately model the coupled near- and far-end voltages between RH and CRLHTLs. Since the equivalent circuit in Fig. 2(b) can be used to accurately model the coupling, the analytical expressions in (17) and (18) can be used to compute the weakly coupled

TABLE II
OPTIMIZED EQUIVALENT CIRCUIT VALUES FOR THE COUPLED RH/CRLHTL UNIT CELLS.

Value	Case 1	Case 2	Case 3
L_R (nH)	2.30	2.30	2.30
C_L (pF)	1.49	1.49	1.08
L_L (nH)	3.14	5.50	5.20
C_R (pF)	1.60	1.60	1.60
L_G (nH)	2.4	2.4	2.4
C_G (pF)	0.92	0.92	0.825
L_{GR} (nH)	0.063	0.063	0.089
C_{GR} (pF)	0.0290	0.0184	0.0114

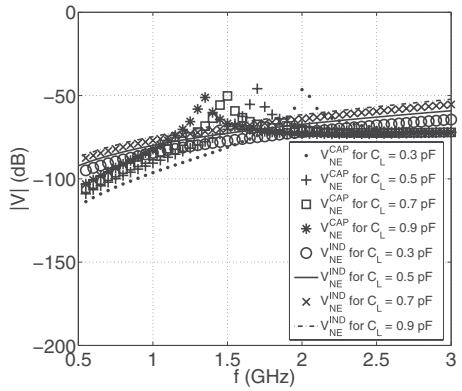

Fig. 11. Near-end voltage due to inductive and capacitive coupling for various values of C_L with $R_L = 2\ \Omega$.

near- and far-end voltages. Also, the same overall agreement was observed for the far-end voltages.

IV. EFFECTS OF C_L AND L_L ON $V_{\rm NE}$ AND $V_{\rm FE}$

To understand the effects of C_L and L_L on the coupled near- and far-end voltages of the CRLHTL, the analytical expressions in (17) and (18) were evaluated. In particular, various values of C_L, L_L, and $R_L = R_{\rm NE} = R_{\rm FE}$ were chosen and the near-end voltage was computed. For the following computations, the equivalent circuit values used in Section II-C were used with the exception of the new values of C_L, L_L, and R_L. Again, this assured that noise voltage was coupled to the receptor in both the LH- and RH-propagating bands.

Initially, the load resistance was defined to be $R_L = 2\ \Omega$. This then satisfied the inequalities reported in [17] for inductively coupled transmission lines at low frequencies. The source was then varied from 0.5 GHz to 3.0 GHz for various values of C_L with L_L fixed at 3.04 nH. The near-end voltages computed for capacitive and inductive coupling using (8) and (15), respectively, are shown in Fig. 11 with the total near-end coupling computed using (17) shown in Fig. 12. The individual near-end voltages due to inductive and capacitive coupling are shown in Fig. 11 to illustrate that inductive coupling is dominant over most of the band and that this contributes mainly to the total coupling. Also, the results in Fig. 12 show that the near-end voltage can be reduced by using lower values of C_L.

Next, C_L was fixed at 0.3 pF and various values of L_L were chosen. The source was again varied from 0.5 GHz to 3.0 GHz.

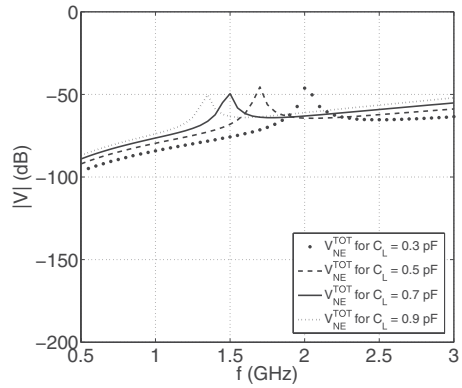

Fig. 12. Total near-end voltage for various values of C_L with $R_L = 2\ \Omega$.

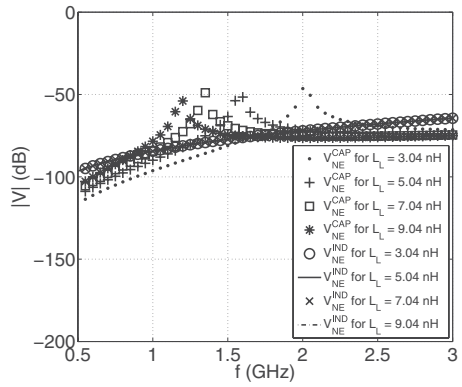

Fig. 13. Near-end voltage due to inductive and capacitive coupling for various values of L_L with $R_L = 2\ \Omega$.

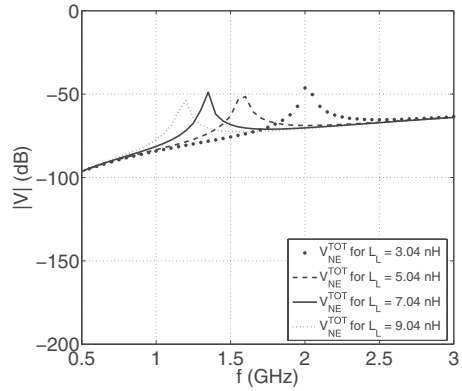

Fig. 14. Total near-end voltage for various values of L_L with $R_L = 2\ \Omega$.

The near-end voltages computed for capacitive and inductive coupling using (8) and (15) are shown in Fig. 13 with the total near-end coupling computed using (17) shown in Fig. 14. Again, the individual near-end voltages due to inductive and capacitive coupling are shown in Fig. 13 to show that inductive coupling is dominant over much of the band; otherwise, capacitive coupling is dominant. The results in Fig. 14 also show that the near-end voltage can be reduced at lower frequencies by using lower values of L_L.

For the next results, the value of R_L was defined to be 34 and 200 Ω. A value of $R_L = 34\ \Omega$ was chosen to result in both a

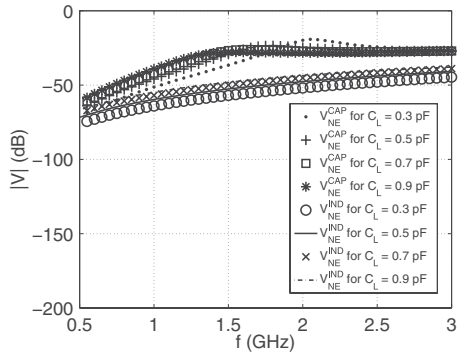

Fig. 15. Near-end voltage due to inductive and capacitive coupling for various values of C_L with $R_L = 34\ \Omega$.

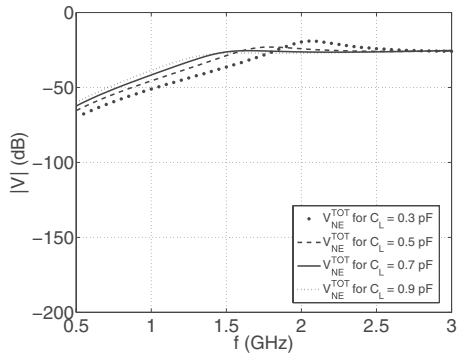

Fig. 16. Total near-end voltage for various values of C_L with $R_L = 34\ \Omega$.

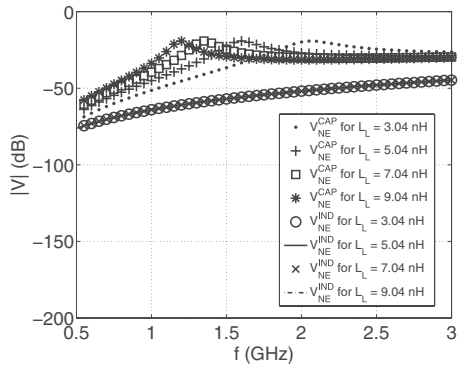

Fig. 17. Near-end voltage due to inductive and capacitive coupling for various values of L_L with $R_L = 34\ \Omega$.

significant inductive and capacitive coupling case and a value of $R_L = 200\ \Omega$ was chosen to provide a case where capacitive coupling was dominant. For $R_L = 34\ \Omega$, the near-end voltages due to coupling are shown in Figs. 15–18. The results in Figs. 15 and 17 are becoming more distinct than the values in Figs. 11 and 13, indicating more of the presence of capacitive coupling. For $R_L = 200\ \Omega$, the near-end voltages due to coupling are shown in Figs. 19–22. The results in Figs. 19 and 21 show that the capacitive coupling is now dominant.

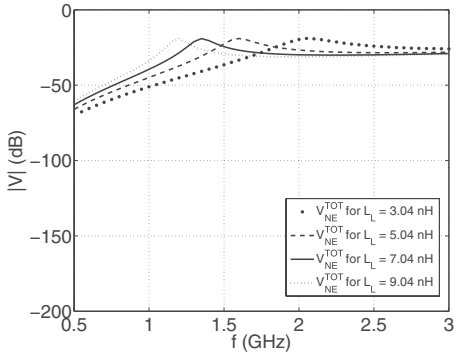

Fig. 18. Total near-end voltage for various values of L_L with $R_L = 34\ \Omega$.

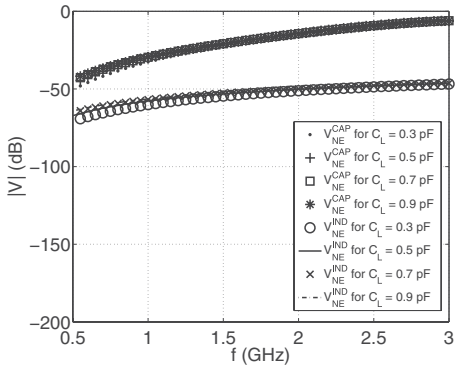

Fig. 19. Near-end voltage due to inductive and capacitive coupling for various values of C_L with $R_L = 200\ \Omega$.

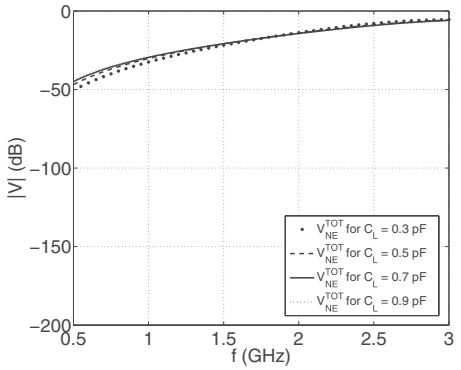

Fig. 20. Total near-end voltage for various values of C_L with $R_L = 200\ \Omega$.

V. Design Tradeoffs, Guidelines and Discussion

A. Coupled Voltages—L_L, C_L Relationship

The results in Figs. 12, 14, 16, 18, 20, and 22 indicate that the near-end voltages can be reduced by reducing the values of both C_L and L_L. There are two ways to illustrate this relationship. First, consider the equivalent circuit in Fig. 2(b) of the coupled RH and symmetric CRLHTL unit cells. By reducing the value of L_L, the impedance of the shunt parallel inductance–capacitance of L_L and C_R will be lower, which increases the current through the impedance. This then decreases the current through $R_{\rm NE}$ and $R_{\rm FE}$, which reduces the unwanted coupled voltages. Similarly, by reducing the value of C_L, the impedance of the LH capacitance will increase. This then reduces the

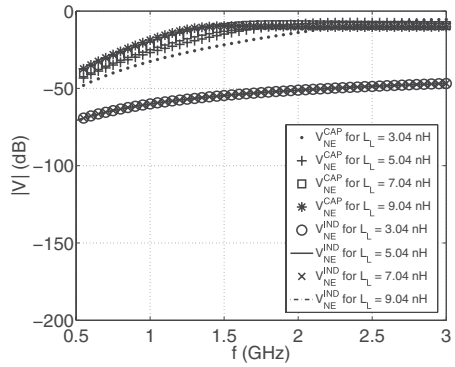

Fig. 21. Near-end voltage due to inductive and capacitive coupling for various values of L_L with $R_L = 200\,\Omega$.

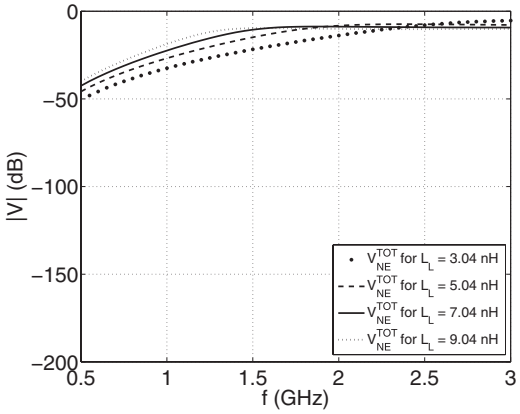

Fig. 22. Total near-end voltage for various values of L_L with $R_L = 200\,\Omega$.

current through $R_{\rm NE}$ and $R_{\rm FE}$, which also reduces the unwanted coupled voltages. A similar observation can be made from the capacitive and inductive coupling models in Fig. 3(a) and (b).

The reduced coupled voltages can also be explained using the analytical expressions in (17) and (18). By decreasing the value of L_L, the parallel impedance Z_P in (5) will be reduced. This then results in an increased value of $Z_{\rm eq}$ in (2) which in turns lowers the capacitively coupled voltage value of V_c in (1). Similarly, by reducing the value of C_L, the near- and far-end impedances in (3) and (4), respectively, are increased. This then reduces the capacitively coupled voltages in (8) and (9). A similar argument can be made for the inductively coupled voltages in (15) and (16).

The results in Figs. 11 and 13 also show that for certain frequencies, inductive coupling is dominant and for others, capacitive coupling is dominant. As described in the previous section, these transition frequencies can be computed using (19) and should be kept in mind during the design process. However, for the results with $R_L = 2\,\Omega$, inductive coupling is dominant for low frequencies, which corresponds to the predictions presented in [17].

B. Tradeoffs Between Reduced Coupled Voltages and the Propagation Characteristics of the CRLHTL

When designing a CRLHTL, several propagation characteristics are of interest. In particular, the lower LH-propagating cutoff frequency $f_{\rm CL}$ of the CRLHTL and the LH-to-RH transition frequency f_0 are considered in a CRLHTL design. The cutoff frequency $f_{\rm CL}$ is the lowest frequency that the CRLHTL will support LH propagation while the frequency value f_0 is the frequency at which the CRLHTL transitions from supporting LH propagation to RH propagation. For the cases studied here, $f_{\rm CL} < f_0$. In general, for a CRLHTL, the lower LH-propagating cutoff frequency can be computed as [1]

$$f_{\rm CL} = f_0\sqrt{\frac{P_1 - P_2}{2}} \tag{20}$$

where

$$P_1 = [K + (2/\omega_L)^2]\omega_0^2 \tag{21}$$

$$P_2 = \sqrt{P_1^2 - 4} \tag{22}$$

$$f_0 = \frac{1}{2\pi\sqrt[4]{L_R C_R L_L C_L}} \tag{23}$$

$$f_L = \frac{1}{2\pi\sqrt{L_L C_L}} \tag{24}$$

and $K = L_R C_L + L_L C_R$. The extracted values in Table II for the weakly coupled transmission lines in Fig. 7 are used to evaluate (20) to compute the lower LH-propagating cutoff frequency for cases 1, 2, and 3. These computations are presented in Table III and it can be observed that by reducing the shunt inductance, as done when comparing cases 2 to 1, the lower LH-propagating cutoff frequency will increase. A similar result can be observed by comparing cases 2 to 3. By reducing C_L to reduce the coupled voltages, the lower LH-propagating cutoff frequency is increased. The values of $f_{\rm CL}$ for cases 1, 2, and 3 are shown in Figs. 8, 9, and 10 for comparison. Similarly, the LH-to-RH transition frequency f_0 was computed using (23) for cases 1, 2, and 3. These values are also shown in Table III and in Figs. 8, 9, and 10 for comparison. As with $f_{\rm CL}$, an increase in the transition frequency can be observed for lower values of L_L and C_L. Therefore, in summary, by reducing the values of L_L and C_L, near- and far-end coupled voltages can be reduced (as shown in Figs. 11–22), which is a useful alternative to conventional shielding; however, the tradeoffs for reducing these coupled voltages are that the frequencies in which the CRLHTL supports LH propagation and the LH-to-RH transition frequency increases.

TABLE III
CUTOFF AND TRANSITION FREQUENCIES FOR THE CRLHTL FOR MEASUREMENT CASES 1, 2, AND 3

Case	$f_{CL}(GHz)$	$f_0(GHz)$
1	1.16	2.47
2	0.879	2.14
3	1.05	2.35

Unintentionally changing the values of $f_{\rm CL}$ and f_0 of a CRLHTL by printing a microstrip RHTL nearby may have the adverse affect of moving the desired LH-operating band of the CRLHTL away from the design frequencies. For example, if a printed conductor is placed near a CRLH-delay line [22], the unintentional coupling can affect the group delay characteristics of the CRLH-delay line. Or if a zero-phase

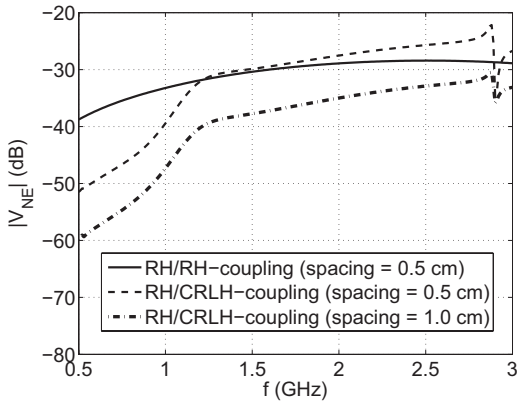

Fig. 23. Total near-end voltage for a spacing of $s = 0.5$ cm and 1.0 cm.

CRLHTL [1] is printed next to a microstrip line, the unwanted coupling can change the zero-phase frequency of the CRLHTL. It has been shown in the previous section that the coupled voltage can be reduced by reducing C_L and L_L. Therefore, if a microstrip is printed next to a CRLHTL-based circuit, the unintentional coupling can be reduced; however, the propagation characteristics (i.e., group delay and zero-phase frequencies) will change.

C. Spacing Design Guidelines for the CRLHTL

Finally, the coupling between the RH and symmetric CRLHTL unit cells in Fig. 2(b) was compared to the coupling between two conventional RHTLs with the same unit cell length and spacing. These problems were investigated in momentum for a spacing of $s = 0.5$ cm and 1.0 cm. The dimensions of each unit cell (both RHTL and CRLHTL) were the same as defined in case 2 in Fig. 7(b). The near-end voltage results from these simulations are shown in Fig. 23. The near-end voltages on the CRLHTL increase above the near-end voltages on the RHTL for a spacing of $s = 0.5$ mm at 1.25 GHz. Comparing this frequency value to the values of f_{CL} and f_0 for case 2 in Table III shows that this transition occurs in the LH-propagating band. Furthermore, the near-end voltages on the CRLHTL are larger than the near-end voltages on the RHTL for frequencies above the transition frequency f_0. To reduce the coupled near-end voltages on the CRLHTL, the separation s was increased to 1.0 cm. The near-end voltages on the CRLHTL for this larger separation are also shown in Fig. 23. This larger separation resulted in near-end voltages on the CRLHTL less than the near-end voltages on the RHTL, indicating that larger separation should be considered when designing a CRLHTL in the proximity of conventional printed microstrip transmission lines.

VI. Conclusion

The weak coupling between a conventional printed transmission line and a CRLHTL has been analyzed from an EMC point of view. New analytical expressions for the coupled near- and far-end voltages on a CRLHTL have been derived and successfully validated with full-wave simulations, circuit modeling, and measurements. It has been shown that unintentional coupled voltages can be reduced by decreasing the values of L_L and C_L along the CRLHTL. This technique could be useful, because reducing L_L and C_L could be used in place of conventional shielding. However, there are tradeoffs between reducing the coupled voltages and the LH-propagation characteristics of the CRLHTL. Design guidelines and a summary of these tradeoffs are discussed in this paper.

References

[1] C. Caloz and T. Itoh, *Electromagnetic Metamaterials: Transmission Line Theory and Applications*. Hoboken, NJ: Wiley, 2006, pp. 86–249.
[2] C. Caloz and T. Itoh, "A novel mixed conventional microstrip and composite right/left-handed backward-wave directional coupler with broadband and tight coupling characteristics," *IEEE Microw. Guided Wave Lett.*, vol. 14, no. 1, pp. 31–33, Jan. 2004.
[3] C. Caloz, A. Sanada, and T. Itoh, "A novel composite right-/left-handed coupled-line directional coupler with arbitrary coupling level and broad bandwidth," *IEEE Trans. Microw. Theory Tech.*, vol. 52, no. 3, pp. 980–992, Mar. 2004.
[4] H. V. Nguyen and C. Caloz, "Generalized coupled-mode approach of metamaterial coupled-line couplers: Coupling theory, phenomenological explanation and experimental demonstration," *IEEE Trans. Microw. Theory Tech.*, vol. 55, no. 5, pp. 1029–1039, May 2007.
[5] H. V. Nguyen and C. Caloz, "First- and second-order differentiators based on coupled-line directional couplers," *IEEE Microw. Wireless Compon. Lett.*, vol. 18, no. 12, pp. 791–793, Dec. 2008.
[6] R. Islam and G. V. Eleftheriades, "Phase-agile branch-line couplers using metamaterial lines," *IEEE Microw. Wireless Compon. Lett.*, vol. 14, no. 7, pp. 340–342, Jul. 2004.
[7] R. Islam, "Theory and applications of microstrip/negative-refractive-index transmission line (MS/NRI-TL) coupled-line couplers" Ph.D. dissertation, Univ. Toronto, Toronto, ON, Canada, 2011.
[8] R. Islam and G. V. Eleftheriades, "Analysis of a finite length microstrip/negative-refractive-index coupled-line coupler," in *Proc. IEEE Antennas Propag. Soc. Int. Symp. Dig.*, Jul. 2005, vol. 1, pp. 268–271.
[9] A. Sanada, C. Caloz, and T. Itoh, "Novel zeroth-order resonance in composite right/left-handed transmission line resonator," in *Proc. Asia-Pacif. Microw. Conf.*, Nov. 2003, pp. 1588–1591.
[10] S. Otto, A. Rennings, C. Caloz, P. Waldow, and T. Itoh, "Composite right/left-handed λ-resonator ring antenna for dual-frequency operation," in *Proc. IEEE Antennas Propag. Soc. Int. Symp.*, Jul. 2005, vol. 1A, pp. 684–687.
[11] C. Caloz, "Metamaterial dispersion engineering concepts and applications," *Proc. IEEE*, vol. 99, no. 10, pp. 1711–1719, May 2011.
[12] A. Sanada, C. Caloz, and T. Itoh, "Characteristics of the composite right/left-handed transmission lines," *IEEE Microw. Wireless Compon. Lett.*, vol. 14, no. 2, pp. 68–70, Feb. 2004.
[13] R. Marques, F. Martin, and M. Sorolla, *Metamaterials With Negative Parameters: Theory, Design and Microwave Applications*. Hoboken, NJ: Wiley, 2008.
[14] N. Engheta and R. W. Ziolkowski, *Metamaterials: Physics and Engineering Explorations*. Hoboken, NJ: Wiley, 2006.
[15] F. Capolino, Ed., *Metamaterials Handbook: Applications of Metamaterials*. Boca Raton, FL: CRC Press, 2009.
[16] G. V. Eleftheriades and K. G. Balmain, *Negative-Refraction Metamaterials: Fundamental Principles and Applications*. Hoboken, NJ: Wiley, 2005.
[17] C. Paul, *Introduction to Electromagnetic Compatibility*. Hoboken, NJ: Wiley, 2006, pp. 599–601.
[18] C. Paul, *Analysis of Multiconductor Transmission Lines*. Hoboken, NJ: Wiley, 1994.
[19] H. W. Ott, *Electromagnetic Compatibility Engeering*. Hoboken, NJ: Wiley, 2009.
[20] *Advanced Design System (ADS) by Agilent Technologies*. (2012). [Online]. Available: www.agilent.com
[21] *Rogers Corporation*. (2012). [Online]. Available:www.rogerscorp.com
[22] S. Abielmona, S. Gupta, and C. Caloz, "Experimental demonstration and characterization of a tunable CRLH delay line system for impulse/continuous wave," *IEEE Microw. Wireless Compon. Lett.*, vol. 17, no. 12, pp. 864–866, Dec. 2007.

Irfanullah (S'05–M'07) received the M.S. degree in electrical engineering from the University of Engineering and Technology, Lahore, Pakistan, in 2007. He is currently working toward the Ph.D. degree in conformal smart antennas at the North Dakota State University, Fargo, ND.

His research interests include the antenna arrays and topics in EMC.

Sanjay Nariyal (S'06) received the B.S. degree in electrical engineering from North Dakota State University, Fargo, ND, in 2010. Currently, he is working toward the M.S. degree in electrical engineering.

He is a Graduate Teaching Assistant in the Electrical and Computer Engineering Department at North Dakota State University. His research interests include antennas and issues in electromagnetic compatibility.

Sayan Roy (S'10) was born in Chandannagar, India, in 1988. He received the B.Tech. degree in electronics and communication engineering from West Bengal University of Technology, Kolkata, India, in 2010 and the M.S. degree in electrical and computer engineering from North Dakota State University, Fargo, ND, in 2012. Currently, he is working toward the Ph.D degree in electrical and computer engineering at North Dakota State University.

His research interests include microwave antennas, printed antenna array, conformal self-adapting antennas, RFID, topics in EMC and wearable antennas.

Muhammad Mubeen Masud received the Masters degree in wireless systems from the Royal Institute of Technology (KTH), Stockholm, Sweden, in 2008. He is currently working toward the Ph.D. degree in the Department of Electrical and Computer Engineering, North Dakota State University, Fargo, ND.

He is an Assistant Professor in Electrical and Computer Engineering Department at COMSATS Institute of Information Technology (CIIT), Lahore, Pakistan and is currently on study leave for his Ph.D. His research interests include printed antennas, antennas for RFID tags, wireless sensors, and topics in EMC.

Bilal Ijaz received the M.Sc. degree in modern digital communication systems from the University of Sussex, U.K., in 2008. He is currently working toward the Ph.D. degree in electrical and computer engineering from North Dakota State University, Fargo, ND.

From 2008 to 2011, he worked as a Faculty Member in the Department of Electrical Engineering at COMSATS Institute of Information Technology, Islamabad, Pakistan. His research activity is focused on antennas, metamaterials and topics in electromagnetic compatibility.

Benjamin D. Braaten (S'02–M'09) received the Ph.D. degree in electrical engineering from North Dakota State University, Fargo, ND, in 2009.

During the 2009 Fall semester he held a post doctoral research position at the South Dakota School of Mines and Technology in Rapid City, SD. Currently, he is an Assistant Professor in the Electrical and Computer Engineering Department at North Dakota State University. His research interests include printed antennas, conformal self-adapting antennas, microwave devices, topics in EMC, and methods in computational electromagnetics.